

Jumps, somersaults, and symmetry breaking in Leidenfrost drops

Simeng Chen and Volfango Bertola

Laboratory of Technical Physics, School of Engineering, University of Liverpool, The Quadrangle, Brownlow Hill L69 3GH, United Kingdom

(Received 15 April 2015; revised manuscript received 18 November 2015; published 16 August 2016)

When a droplet of water impacts a heated surface, the drop may be observed to bounce. Recently it has been found that small quantities (~ 100 ppm) of polymer additives such as polyethylene oxide can significantly increase the maximum bouncing height of drops. This effect has been explained in terms of the reduction of energy dissipation caused by polymer additives during the drop retraction and rebound, resulting in higher mechanical energy available for bouncing. Here we demonstrate, by comparing three types of fluids (Newtonian, shear-thinning, and viscoelastic), that the total kinetic energy carried by low-viscosity Newtonian drops during retraction is partly transformed into rotational kinetic energy rather than dissipated when compared with high-viscosity or non-Newtonian drops. We also show that non-Newtonian effects play little role in the energy distribution during drop impact, while the main effect is due to the symmetry break observed during the retraction of low-viscosity drops.

DOI: [10.1103/PhysRevE.94.021102](https://doi.org/10.1103/PhysRevE.94.021102)

When a liquid droplet impacts on a high-temperature surface, one may observe bouncing back of the droplet off the surface due to the creation of a thin vapor film between the drop and surface upon impact. This phenomenon is known as “dynamic Leidenfrost phenomenon” [1–3], and is encountered in various industrial applications including spray cooling, fire suffocation [4], and spray quenching [5]. So far, research efforts to understand the Leidenfrost phenomenon were mainly focused on Newtonian fluids such as water [6,7]. However, there is a growing interest in non-Newtonian drops because of their role in food, cosmetics, and biopharmaceutical industries, among others. Thus a better understanding of Leidenfrost drop impact behaviors of both Newtonian and non-Newtonian fluids and the physical mechanisms behind them is necessary to improve such industrial processes.

The impact morphology of Leidenfrost drops is relatively simple: upon impact, the drop spreads over the vapor film in a short time (about 5 ms); after maximum spreading, two different outcomes are possible depending on the impact velocity, the fluid properties, and the surface temperature. For high impact kinetic energies, the drop will disintegrate into smaller droplets; otherwise, it will recoil under the action of surface forces, to minimize the surface energy, and eventually bounce off the surface if there is sufficient kinetic energy at the end of the recoil. The drop impact dynamics is characterized by competition between inertial and capillary forces, represented by the dimensionless Weber number $We = \rho v_z^2 D_0 / \sigma$, where ρ is the fluid density, v_z denotes the vertical impact velocity, and D_0 denotes the equilibrium drop diameter prior to impact. However, drops of viscous fluids can dissipate rather than convert most of their kinetic energy on impact. To account for viscous effects, one can introduce the Reynolds number $Re = \rho v_z D_0 / \mu$, representing the ratio of inertial to viscous forces, and the Ohnesorge number $Oh = \sqrt{We}/Re$, representing the ratio of viscous to capillary forces, where μ is the shear viscosity of the fluid. Rebound is eased by the vapor film [8], which acts as a lubricant layer, reducing frictional energy dissipation during both the initial inertial spreading of the drop and the following recoil. Since the liquid is not in contact with the surface, bouncing Leidenfrost drops represent a unique model system to investigate the dynamics

of drop impact independently of wetting and contact angle hysteresis [9,10]. In particular, the energy dissipation during the whole impact process and rebound can be easily calculated as the difference between the gravity potential energies of the drop when it is released at its initial position above the target surface and when it reaches the maximum bouncing height.

Recently, it has been found that small quantities (~ 100 ppm) of polymer additives such as polyethylene oxide can significantly increase the maximum bouncing height of drops at relatively high Weber numbers ($We \sim 100$) [10–12]. It has been suggested that this effect may be due to a reduction of energy dissipation during the drop retraction and rebound, resulting in higher mechanical energy for bouncing in the case of non-Newtonian drops. This is surprising because the apparent shear viscosity of a polymer solution is higher than that of the solvent. However, it was also observed that the retraction velocity of non-Newtonian drops is of the same order of magnitude as water drops [10]; if there was a significant reduction of energy dissipation during the retraction stage, one would expect to see an increased velocity.

In the present work, we show that frictional energy dissipation and non-Newtonian effects do not explain the higher rebounds observed in polymer solutions, but the bouncing height differences are likely to be caused by a redistribution of mechanical energy among the different degrees of freedom of the drop. Our experimental results enable us to find a reasonable physical mechanism which explains why low-viscosity Newtonian drops bounce much lower than high-viscosity Newtonian or non-Newtonian drops in the Leidenfrost regime. This is achieved by comparing the virtual maximum bouncing height (calculated by transforming rotational kinetic energy into additional potential energy) of low-viscosity Newtonian drops with the maximum bouncing height of high-viscosity Newtonian and non-Newtonian drops with the same rheology. The top view images of the retracting droplet show “fingers” developing on the rim surrounding the lamella, which may coalesce to create nonaxisymmetric flow, resulting in a rotation of low-viscosity Newtonian drops at high impact We numbers.

To disentangle different non-Newtonian effects, model fluids with different rheological behavior (Newtonian, shear-thinning, and viscoelastic) were prepared by

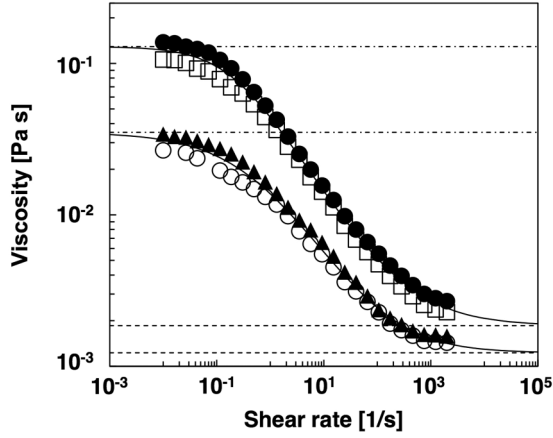


FIG. 1. Flow curves of the model fluids measured with an MCR302 rheometer (Anton Paar) equipped with a cone-plate geometry (75 mm diameter; 2° angle): \circ , 100 ppm XG; \blacktriangle , 80 ppm PAA, \square , 400 ppm XG, and \bullet , 300 ppm PAA. Solid lines represent the Carreau-Yasuda model fit curves of the average values of measured XG and PAA data. Dashed lines and dot-dashed lines indicate the constant viscosities of GLY with infinite-shear viscosity and GLY with zero-shear viscosity, respectively.

dissolving in deionized water (Barnstead Easypure) glycerol ($\rho = 1250 \text{ kg/m}^3$), xanthan gum ($\rho = 1500 \text{ kg/m}^3$; average MW = 4×10^6 to 12×10^6 Da), and polyacrylamide ($\rho = 1130 \text{ kg/m}^3$; average MW = 27×10^6 Da), respectively. While xanthan gum (XG) solutions are purely shear thinning, polyacrylamide (PAA) solutions exhibit both shear-thinning and viscoelastic behaviors; to isolate viscoelastic effects, polymer concentrations were adjusted to obtain fluids with matching flow curves, as shown in Fig. 1. Flow curves were fitted with the Carreau-Yasuda model, to obtain the values of the zero-shear viscosity (μ_0) and infinite-shear viscosity (μ_∞):

$$\mu_{CY} = \mu_\infty + (\mu_0 - \mu_\infty) / [1 + (\lambda_{CY}\dot{\gamma})^a]^{n/a}. \quad (1)$$

Finally, Newtonian glycerol solutions (GLY) were prepared with viscosities equal to the zero-shear viscosity (μ_0) and infinite-shear viscosity (μ_∞) of the corresponding XG and PAA solutions.

In the case of Leidenfrost drops, the vapor film between the drop and the surface removes the no-slip boundary condition, therefore the velocity gradient in the vertical direction is likely to be very small. As a consequence, the rate of shear will be small, and the relevant part of the flow curves will be near the zero-shear rate.

Drops with an equilibrium diameter of ~ 3 mm were generated using a blunt hypodermic (gauge 21, i.d. 0.495 mm) and impacted on a polished aluminum surface, kept at the temperature of 400°C . Temperature could be controlled within $\pm 1^\circ\text{C}$ by a PID controller driven by a K thermocouple placed 1 mm below the point of impact. This temperature is high enough to keep the vapor film stable and avoid the formation of secondary droplets [13]. Adjusting the position of the dispensing needle with a digital height gauge allowed changing the impact velocity, hence the impact Weber number. A detailed description of the experimental setup can be found in [10].

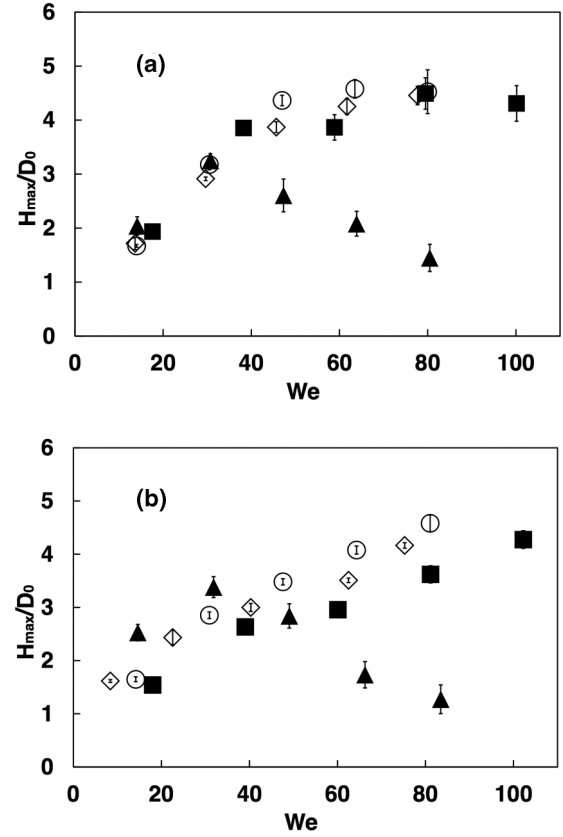


FIG. 2. Maximum bouncing height of the drops normalized with respect to the equilibrium drop diameter of model fluids as a function of the impact Weber number: (a) \circ , 100 ppm XG; \diamond , 80 ppm PAA; \blacktriangle , GLY with infinite-shear viscosity, and \blacksquare , GLY with zero-shear viscosity. (b) \circ , 400 ppm XG; \diamond , 300 ppm PAA; \blacktriangle , GLY with infinite-shear viscosity, and \blacksquare , GLY with zero-shear viscosity.

Figure 2 displays the normalized maximum bouncing height of XG, PAA, and the matching GLY drops as a function of the impact Weber number. The maximum bouncing height (H_{\max}) denotes the maximum height reached by the drop center of mass during rebound. Under certain conditions satellite drop(s) may be created during rebound [see Fig. 3(a)], therefore the corresponding reported data in Fig. 2 were corrected by taking the kinetic energy of satellite drop(s) into account. As shown in Fig. 2(a), the maximum bouncing heights of 100 ppm XG, and 80 ppm PAA and GLY with zero-shear viscosity drops are almost consistent in the considered Weber number range. It can also be observed that the maximum bouncing height tends to reach a constant value at high Weber numbers for these three fluids. However, the maximum bouncing height of GLY with infinite-shear viscosity drops starts to decrease at a critical Weber number ~ 30 . Coincidentally, this feature can also be seen in a higher concentration case with the same critical Weber number as shown in Fig. 2(b). One may conclude that the GLY with infinite-shear viscosity drops (i.e., those with the lowest viscosity) are subjected to large energy dissipation during impact, which leads to less potential energy restored when reaching maximum height.

Interestingly, the bouncing drops of glycerol with infinite-shear viscosity were observed to “somersault” beyond this

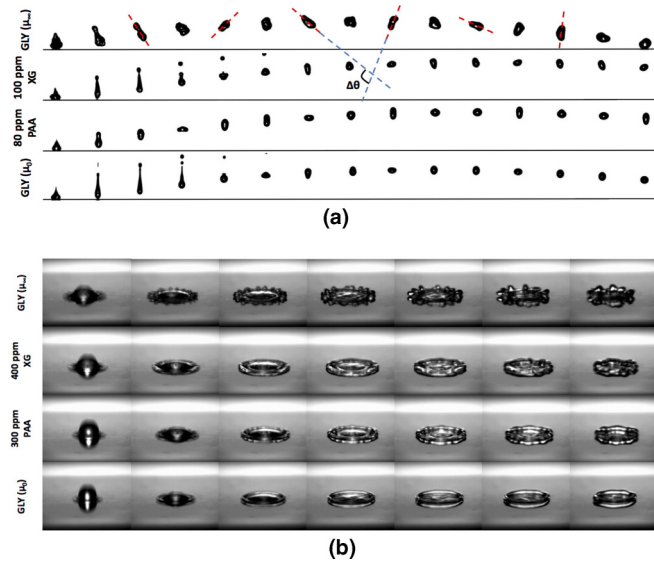


FIG. 3. (a) Rebound morphology of Leidenfrost drops of different model fluids at $We \approx 70$. The time between two consecutive images is 5 ms. (b) Spreading and retracting morphology of Leidenfrost drops of different model fluids at $We \approx 70$. The time between two consecutive images is 1 ms.

critical Weber number (~ 30) and no distinct rotational motion can be observed below this critical Weber number for all the other types of drops. Figure 3(a) shows the rebound morphology of Leidenfrost drops of different model fluids at $We \approx 70$. It can be clearly seen that the GLY with infinite-shear viscosity drops rotate during rebound, while drops of the other three model fluids exhibit only symmetric oscillations in the direction of rebound [see Supplemental Material video 1 (rotating drop) and video 2 (nonrotating drop) [14]]. The dashed red lines parallel to the stretching direction of the bouncing drops in the first row of images in Fig. 3(a) approximately represent the transient vibrational direction of the bouncing drops, while the vibrational directions of the other three types of drops remain almost vertical. Thus, the angular velocity of the rotating drops can be roughly estimated as the ratio of the angle of rotation in two images over the time between the images: $\omega = \Delta\theta/\Delta t$. In general, this introduces an error because the rotation angle is measured in the plane of the field of view, while the actual rotation occurs in a three-dimensional space; however, the error can be removed provided the rotation angle is measured taking reference points on the axes of an orthogonal Cartesian coordinate system (for example, the angle corresponding to one revolution, $\Delta\theta = 2\pi$, remains the same for any reciprocal position of the rotation plane and the field of view). Thus, there is only one case where the angular velocity is not measurable, that is, when the rotation is exactly in the plane perpendicular to the field of view.

The calculated values of mean angular velocities of infinite-viscosity GLY drops are displayed in Fig. 4 for Weber numbers beyond ~ 30 (critical We). The overall result of this complex oscillation dynamics is that the drop center of mass does not move along the same vertical trajectory during drop rebound, but combines the vertical, ascending movement

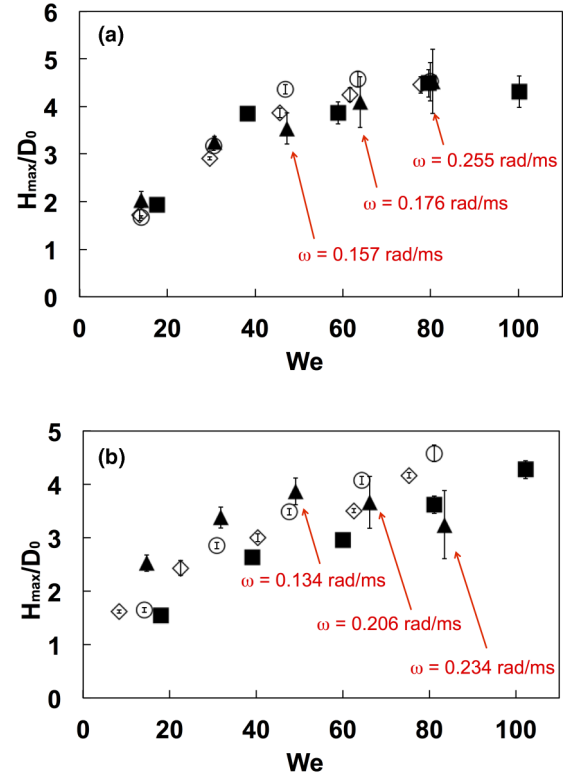


FIG. 4. Maximum bouncing height (modified data for GLY with infinite-shear viscosity) of the drops normalized with respect to the equilibrium drop diameter of model fluids as a function of the impact Weber number: (a) \circ , 100 ppm XG; \diamond , 80 ppm PAA; \blacktriangle , GLY with infinite-shear viscosity, and \blacksquare , GLY with zero-shear viscosity. (b) \circ , 400 ppm XG; \diamond , 300 ppm PAA; \blacktriangle , GLY with infinite-shear viscosity, and \blacksquare , GLY with zero-shear viscosity. Error bars represent the mean square value of the errors on the center of mass height and on the virtual lengths obtained from Eq. (4).

with a rotational movement of smaller amplitude. The energy associated with the drop dynamics must be independent of the reference frame; thus, we estimate this energy in a reference frame moving with the drop center of mass, as if the drop was rotating instead of oscillating. In order to estimate the rotational kinetic energy of the tumbling drops we use the moment of inertia of a solid cylinder as an approximation, although the shape of the bouncing drop is changing due to vibration:

$$I = m \left(\frac{R^2}{4} + \frac{l^2}{12} \right) = \frac{1}{72} \pi \rho D_0^5 \left(\frac{1 + 2k^3}{2k} \right), \quad (2)$$

where $l = kD_0$ is the cylinder length, measured from images, and R is the cylinder radius, calculated imposing volume conservation. By inserting the moment of inertia into Eq. (2) the rotational kinetic energy can then be expressed as

$$E_{\text{rot}} = \frac{1}{2} I \omega^2 = \frac{1}{144} \pi \rho \omega^2 D_0^5 \left(\frac{1 + 2k^3}{2k} \right). \quad (3)$$

The increment in maximum bouncing height (normalized with respect to the equilibrium drop diameter) if all the rotational kinetic energy was converted into potential energy can be

written as

$$\frac{\Delta h}{D_0} = \frac{E_{\text{rot}}}{mgD_0} = \frac{D_0\omega^2}{24g} \left(\frac{1+2k^3}{2k} \right), \quad (4)$$

where ω denotes the mean angular velocity, and g the gravity acceleration.

If $\Delta h/D_0$ defined by Eq. (4) is added to the original maximum bouncing height data of the infinite-viscosity GLY drops for Weber numbers higher than ~ 30 , a new graph which displays the normalized maximum bouncing height of XG, PAA, and the matching GLY drops with respect to the equilibrium drop diameter as a function of the impact Weber number can be plotted (see Fig. 4).

It is important to observe that the measured angular velocities are in quantitative agreement with the shape oscillation frequencies reported in [12], which confirms that the drop rotation in the relative coordinate system corresponds to nonsymmetric drop oscillations and deformations in a fixed reference frame.

The fact that the “virtual maximum bouncing height” of infinite-viscosity GLY drops is consistent with the measured maximum bouncing height of other types of drops indicates that the total kinetic energy carried by low-viscosity Newtonian drops during retraction is only partly transformed into rotational kinetic energy rather than dissipated. The small difference of maximum bouncing height between Newtonian and non-Newtonian drops in Fig. 4(b) implies that non-Newtonian effects play little role in the energy distribution.

To investigate the physical mechanism of symmetry break (i.e., why some drops exhibit symmetric oscillations during rebound, and others do not), the high-speed camera was inclined with respect to the impact surface with an angle of $\sim 20^\circ$ in order to view the morphology of spreading and retracting drops from the top [see Fig. 3(b)]. One can observe distinct fingerlike protrusions on the rim in the case of GLY

with infinite-shear viscosity drops at Weber numbers beyond ~ 30 , which indicate the onset of the well-known rim instability eventually leading to splashing. Similar disturbances on the rim are also observed for drop impact onto a solid surface [15] and, as is well known, they become more pronounced in the case of low-viscosity fluids [15,16]. These protrusions grow during the inertial spreading stage, and form an axisymmetric crown at maximum spreading; however, at the onset of recoil one can observe that some of the protrusions coalesce to create bigger fingers during retraction, while others do not. This is likely to be caused by another instability of the rim, which can be modeled as a toroidal ring subject to radial compression. Thus, the mass distribution in the retracting droplet becomes nonuniform, which induces asymmetries both in the drop shape and in the internal flows, and eventually causes the drop to rotate during rebound (see Supplemental Material [14] for a video of the generation of asymmetry).

In conclusion, our work demonstrates that the total kinetic energy carried by low-viscosity Newtonian drops during retraction is partly transformed into rotational kinetic energy rather than dissipated when compared with high-viscosity or non-Newtonian drops. By comparing the virtual maximum bouncing height (calculated by transforming rotational kinetic energy into extra potential energy) and top view images in the retraction phase of low-viscosity Newtonian drops with those of high-viscosity Newtonian and non-Newtonian drops, we showed that the somersault effect is due to the symmetry break observed during the retraction of low-viscosity drops.

Note added. We recently became aware of a paper where a very similar approach is used to investigate drop tumbling on an inclined plate [17]; that paper also includes lattice Boltzmann simulations showing that tumbling is due to the internal angular velocity of the fluid, which justifies the analogy with a tumbling solid body.

-
- [1] L. Wachters and N. Westerling, *Chem. Eng. Sci.* **21**, 1047 (1966).
 - [2] D. Quéré, *Annu. Rev. Fluid Mech.* **45**, 197 (2013).
 - [3] A.-L. Bianco, F. Chevy, C. Clanet, G. Lagubeau, and D. Quéré, *J. Fluid Mech.* **554**, 47 (2006).
 - [4] G. Grant, J. Brenton, and D. Drysdale, *Prog. Energy Combust. Sci.* **26**, 79 (2000).
 - [5] J. D. Bernardin and I. Mudawar, *Int. J. Heat Mass Transfer* **38**, 863 (1995).
 - [6] J. D. Bernardin and I. Mudawar, *J. Heat Transfer* **126**, 272 (2004).
 - [7] A. Moreira, A. Moita, and M. Panao, *Prog. Energy Combust. Sci.* **36**, 554 (2010).
 - [8] J. C. Burton, A. L. Sharpe, R. C. A. van der Veen, A. Franco, and S. R. Nagel, *Phys. Rev. Lett.* **109**, 074301 (2012).
 - [9] Z. Yu, F. Wang, and L.-S. Fan, *Ind. Eng. Chem. Res.* **47**, 9174 (2008).
 - [10] V. Bertola, *Int. J. Heat Mass Transfer* **52**, 1786 (2009).
 - [11] K. Black and V. Bertola, *Atomization Sprays* **23**, 233 (2013).
 - [12] V. Bertola, *Exp. Thermal Fluid Sci.* **52**, 259 (2014).
 - [13] V. Bertola, *Int. J. Heat Mass Transfer* **85**, 430 (2015).
 - [14] See Supplemental Material at <http://link.aps.org/supplemental/10.1103/PhysRevE.94.021102> for rotating and nonrotating drop videos, along with an asymmetry generation video.
 - [15] M. Rein, *Fluid Dyn. Res.* **12**, 61 (1993).
 - [16] A. Yarin, *Annu. Rev. Fluid Mech.* **38**, 159 (2006).
 - [17] C. Antonini, S. Jung, A. Wetzel, E. Heer, P. Schoch, A. M. Moqaddam, S. S. Chikatamarla, I. Karlin, M. Marengo, and D. Poublikakos, *Phys. Rev. Fluids* **1**, 013903 (2016).